Rotating Switching Surface Control of Series-Resonant Converter Based on a Piecewise Affine Model

Mohammad Momeni, Homayoun Meshgin Kelk, and Heidarali Talebi, *Senior Member, IEEE*

***Abstract*—In this paper, the control signal of the series-resonant converter is considered as a slope of a switching surface. The output characteristic of the converter, for an ideal case and above the resonant frequency, is achieved based on the slope of the switching surface. This output characteristic leads us to find the related slope for a specific converter gain. Nonlinear state equations of the series-resonant converter with new control input are represented in widely used class of hybrid systems that have been called piecewise affine systems. Considering the effects of the slope variations in the switching surface, a simple and efficient control law is achieved. The main advantage of the proposed method is the absence of microcontroller and frequency modulator integrated circuits in hardware implementation. This property makes the proposed method more beneficial in high-frequency applications. Experimental results confirm our theoretical investigations.**

***Index Terms*—Piecewise affine system, series-resonant converter, switching surface.**

I. Introduction

DUE to the development of technology, efficiency and switching loss in power electronic converters have received a great deal of attention. In recent years, the resonant converters with suitable properties of zero voltage switching (ZVS) and zero current switching, low electromagnetic interferences, and high-frequency operation are investigated in many research works [1].

Unlike pulse width modulation (PWM) converters, some state variables of the resonant converters are quasi-sinusoidal with zero mean value signals in steady state. These properties enable us to simplify the nonlinear model of the resonant converters in two steps: harmonic approximation and averaging over a switching period. The small-signal model of the converter could be achieved with linearization of the simplified model around the operational point [2], [3]. Because of the first harmonic approximation, the simplified model does not possess enough accuracy to model all behavior of the nonlinear system. Indeed, the first harmonic approximation can be just used for the resonant converter with large quality factor [4].

Manuscript received December 20, 2013; revised March 30, 2014; accepted May 6, 2014. Date of publication May 19, 2014; date of current version October 15, 2014. Recommended for publication by Associate Editor M. Ferdowsi.

M. Momeni and H. M. Kelk are with the Department of Electrical Engineering, Tafresh University, Tafresh 39518-79611, Iran (e-mail: m_momeni_65@yahoo.com; meshgin@tafreshu.ac.ir).

H. Talebi is with the Department of Electrical Engineering, Amirkabir University of Technology, Tehran 15914, Iran (e-mail: alit@aut.ac.ir).

Color versions of one or more of the figures in this paper are available online at http://ieeexplore.ieee.org

Digital Object Identifier 10.1109/TPEL.2014.2325641

State variables of the resonant converters such as capacitor voltage and inductor current are continuous variables. However, switches operate in a discrete pattern. Such a system belongs to a set of control systems called hybrid systems [5]. Modeling and control of PWM converters is considered in [6] and [7] by hybrid control approach. Piecewise affine (PWA) systems are an important class of hybrid systems which are used to model many nonlinear systems [5]. PWA approximation for averaged models of PWM converters has been presented in [8]. In [9], a hybrid model for series-resonant converters is introduced, which applies the first harmonic approximation to compute the switching surface slope. Moreover, the slope of the switching surface is considered as an unknown parameter that can be found by solving the system stability problem with different results for different convergence conditions on the Lyapunov function [9], which do not reflect the exact specific gain.

The nonlinear nature of the resonant converters makes the control of this class of power electronic converters so attractive. An adaptive control approach has been considered to control the series-resonant converter in which a personal computer (PC) and a digital signal processor were used for the realization of the closed-loop system developed based on complicated mathematical relations [10]. An asymmetrical voltage cancelation approach has been developed in [11] based on first harmonic approximation for resonant-tank state variables. The integration of the control signal as a combination of the resonant frequency and its subharmonics is discussed in [12]. The approach proposed in [12] needs to compute absolute and sign value of resonant-tank current and voltage. The autoswitching method for driving power switch in an LED driver system is proposed in [13], where a feedback from resonant inductor current has been employed to regulate the output voltage. In [14], a variable magnetic approach with a traditional compensator has been applied to control the series-resonant converter where the output voltage of the converter has unsuitable underdamped response.

In this study, the phase plane of the series-resonant converter is analyzed. Based on the phase-plane analysis, the definitions of the switching surface parameters and the effect of switching surface parameter variations on the converter gain are also studied. The main contribution of this paper is looking at output characteristic of the series-resonant converter based on the switching surface slope. A model of the series-resonant converter with switching surface is represented in the PWA class of the hybrid systems. Furthermore, this paper proposes a simple and effective control law, based on the performed analysis from switching surface rotation effect on the converter behavior, for

output voltage regulation against load changes, input voltage variations, and reference voltage tracking. The simplicity of the control law causes the closed-loop system to be applicable in high switching frequencies.

This paper is organized as follows. In Section II, a brief description of the series-resonant converter is presented. Section III offers a procedure to define the switching surface slope for a specific voltage gain and series-resonant converter PWA model. Section IV presents the control law for output voltage regulation, and finally, Section V illustrates the experimental results.

II. Principle of the Series-Resonant Converter

The series-resonant converter is assumed to be in continuous conduction mode (CCM) and is operating above resonance. Moreover, it is assumed that all components are ideal and the output filter capacitor is large enough to keep the output voltage constant through a switching period. In Fig. 1, a series-resonant converter is illustrated which consists of an input voltage source V_g, a full-bridge inverter, a series-resonant tank, a full-bridge rectifier, and a load that includes a resistor R and a capacitor C_F. Controllable switches Q_1, Q_2, Q_3, and Q_4 with their antiparallel diodes D_1, D_2, D_3, and D_4 provide a square wave $v_S(t)$ in the series-resonant-tank input terminal. The amplitude of the resonant current and, as a result, the output voltage $v(t)$ could be controlled by frequency control of $v_S(t)$. Steady-state waveforms of a series-resonant converter are plotted in Fig. 2.

A state-space representation of the system could be written as

$$\begin{aligned}\frac{d}{dt}i_L(t) &= \frac{1}{L}\{V_g u(t) - v(t)\text{sign}(i_L(t)) - v_C(t)\}\\ \frac{d}{dt}v_C(t) &= \frac{1}{C}i_L(t)\\ \frac{d}{dt}v(t) &= \frac{1}{C_F}\left\{|i_L(t)| - \frac{v(t)}{R}\right\}\end{aligned} \tag{1}$$

where $i_L(t)$, $v_C(t)$, and $v(t)$ are inductor current, resonant-tank capacitor voltage, and output voltage, respectively. The control input of the system is $u(t)$, which is limited to take values in the set $\{-1, +1\}$. Defining normalized state space and time transformation

$$\begin{bmatrix} x_1 \\ x_2 \\ x_3 \end{bmatrix} = \begin{bmatrix} \frac{1}{V_g}\sqrt{\frac{L}{C}} & 0 & 0 \\ 0 & \frac{1}{V_g} & 0 \\ 0 & 0 & \frac{1}{V_g} \end{bmatrix} \begin{bmatrix} i_L \\ v_C \\ v \end{bmatrix}, \tau = \frac{t}{\sqrt{LC}} \tag{2}$$

the result is a normalized state-space model of the series-resonant converter

$$\begin{aligned}\dot{x}_1 &= u - x_3\text{sign}(x_1) - x_2\\ \dot{x}_2 &= x_1\\ \alpha\dot{x}_3 &= |x_1| - x_3 Q\end{aligned} \tag{3}$$

where x_1, x_2, and x_3 are the normalized inductor current, normalized resonant capacitor voltage, and normalized output voltage, respectively. Furthermore, the symbol "$\bullet$" represents derivation with respect to the scaled time τ and $\alpha = C_F/C$. The quality factor, characteristic impedance, and resonant angular frequency of the converter are defined as $Q = Z/R$, $Z = \sqrt{L/C}$, and $\omega_o = 1/\sqrt{LC}$, respectively [15].

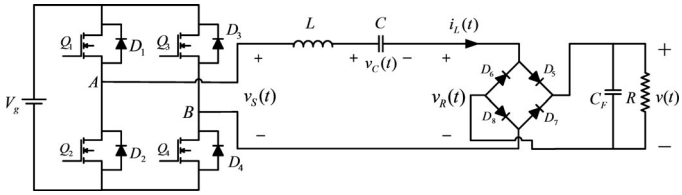

Fig. 1. Series-resonant converter circuit.

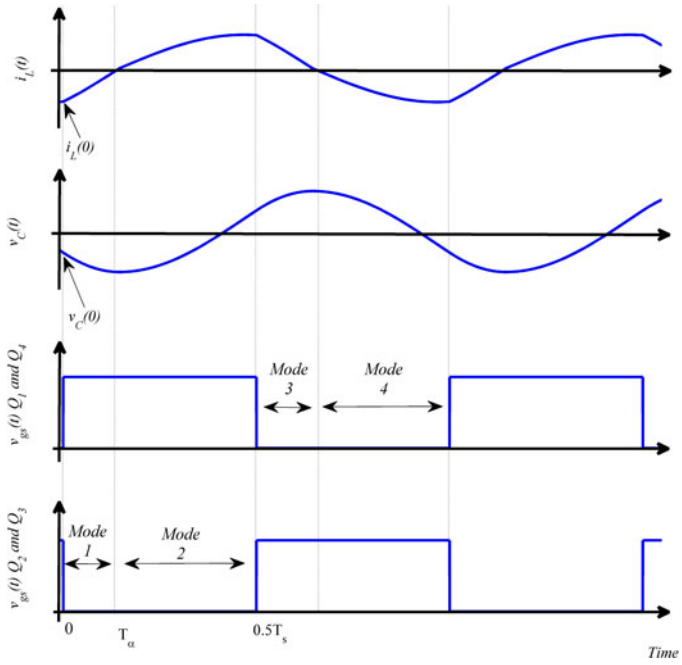

Fig. 2. Steady-state signals of a series-resonant converter in CCM and above resonance.

In the above resonance, the ZVS phenomenon can occur and every switching period could be divided into four subintervals. In the first subinterval (*Mode 1*), associated with Fig. 3(a), switches Q_1 and Q_4 have been turned ON and the inductor current is negative which causes the current flow through the parallel diodes D_1 and D_4. When inductor current becomes positive, *Mode 2* will be started and switches Q_1 and Q_4 conduct. The equivalent circuit of this mode is plotted in Fig. 3(b). At the time instant $t = T_s/2$, switches Q_1 and Q_4 will be turned OFF and *Mode 3* is started. The waveforms for *Mode 3* and *Mode 4* are symmetrical to the ones for *Mode 1* and *Mode 2*, respectively.

The output characteristic of the series-resonant converter for above resonance operation could be described as [1]

$$x_{3ss}^2 \sin^2\left(\frac{\gamma}{2}\right) + \left(\frac{x_{3ss}Q\gamma}{2} + 1\right)^2 \cos^2\left(\frac{\gamma}{2}\right) = 1,$$

$$\gamma = \frac{\omega_o T_s}{2} \tag{4}$$

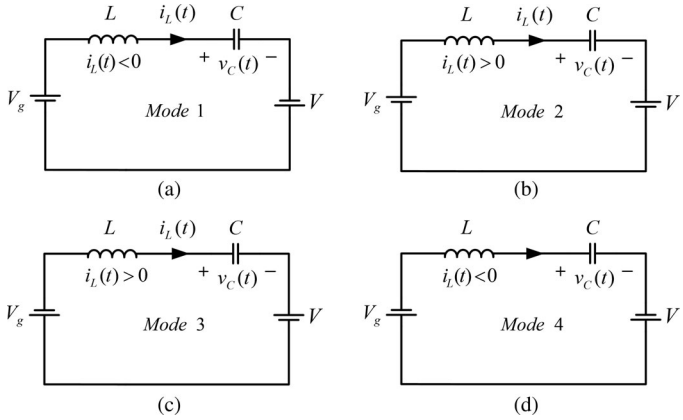

Fig. 3. Equivalent circuits of series-resonant converter operational modes in CCM and above resonance.

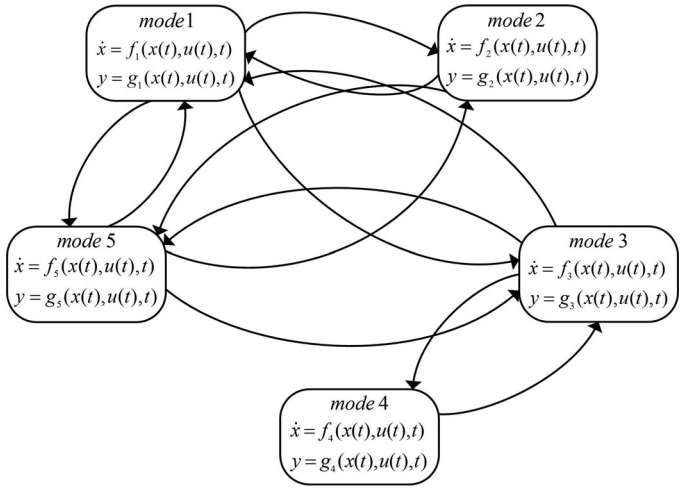

Fig. 4. Hybrid system with five modes.

where T_s is the switching period and $x_{3ss} = V/V_g$.

It is clear that the system has nonlinear behavior which models the effects of controllable and uncontrollable switches. The sign and the absolute value in the normalized state-space model of the system in (3) mathematically explain these effects. A common method in simplifying model (3) is the generalized state-space averaging described in [3]. Using this method, a new linearizable state-space model can be achieved. Moreover, these new state variables of the model could be obtained by the first harmonic approximation of the inductor current or the capacitor voltage of the resonant tank and dc component approximation of the output voltage. Due to neglecting fast dynamics, the model given by this method shows low level of precision and its application is constrained by the quality factor of the system [1], [4].

III. Series-Resonant Converter PWA Modeling

In this section, a brief description of hybrid dynamical and PWA systems is presented, and then, the PWA model of the series-resonant converter is derived. A simple description of hybrid systems has been reported by Witsenhausen [16]. A system with different operation modes in which every mode has its difference or differential equations is called a hybrid system. The system mode will be changed when an event happens (see Fig. 4). In a hybrid system, an event can occur based on different reasons such as elapse of time interval, exogenous inputs, state variables value, etc. A mathematical representation for a continuous time hybrid system can be written as

$$\begin{aligned} \dot{x}(t) &= f_{\sigma(t)}(x(t), u(t), \omega(t)) \\ y(t) &= g_{\sigma(t)}(x(t), u(t), \omega(t)) \\ \sigma(t^+) &= \sigma(t, \omega(t), x(t)/y(t), z(t)) \end{aligned} \tag{5}$$

where $x(t)$, $u(t)$, $\omega(t)$, $\sigma(t)$, and $z(t)$ are state vector, control input, disturbance input, subsystem indicator, and exogenous input, respectively [5].

PWA systems are a class of hybrid systems to model nonlinear systems. These systems have continuous states and their switch constraints are related to state variables. Dynamic equations of a PWA system have the form of

$$\begin{cases} \dot{x} = A_i x + B_i u(t) + b_i \\ y = C_i x \end{cases} \tag{6}$$

where $x \in \Re^n$, $u \in \Re^m$, and $b_i \in \Re^n$ are state vector, input vector, and a constant vector, respectively [17]. This dynamic equation corresponds to a partition of the state space which is constructed as the intersection of finite number (p_i) of half spaces with the following description [18]:

$$\Re_i = \left\{ x \middle| \, H_i^T x - g_i < 0 \right\} \tag{7}$$

$$H_i = [h_{i1} \;\; h_{i2} \;\; \cdots \;\; h_{ip_i}], \quad g_i = [g_{i1} \;\; g_{i2} \;\; \ldots \;\; g_{ip_i}]^T. \tag{8}$$

As can be seen from the dynamics of the series-resonant converter in (3), this system has two kinds of events. Discrete functions $\mathrm{sign}(x_1(\tau))$ and $u(\tau)$ indicate the state-event and the time-event of the system, respectively. On the other hand, to model the system in the PWA class, it is appropriate to describe $u(\tau)$ as a discrete function of the state variable. In this way, $u(\tau)$ can be considered as a sign function of a surface in the state space of the system $\Re^3$

$$u(\tau) = \mathrm{sign}(S), S = \begin{bmatrix} 1 & -k_n & -k_m \end{bmatrix} \begin{bmatrix} x_1 \\ x_2 \\ x_3 \end{bmatrix} = 0 \tag{9}$$

where k_m and k_n are real coefficients and must be defined. The state trajectory of a series-resonant converter with normalized dynamics (3) is plotted in Fig. 5. With the assumption of constant output voltage and negligible ripple on this signal, k_m can be neglected. Moreover, in this situation, the dynamics of the system can be reduced to

$$\begin{bmatrix} \dot{x}_1 \\ \dot{x}_2 \end{bmatrix} = \begin{bmatrix} 0 & -1 \\ 1 & 0 \end{bmatrix} \begin{bmatrix} x_1 \\ x_2 \end{bmatrix} + \begin{bmatrix} u(\tau) - x_{3ss}\mathrm{sign}(x_1) \\ 0 \end{bmatrix}. \tag{10}$$

The reduced-system phase-plane trajectory could be obtained using (10) as shown in Fig. 6. In Fig. 6, the locations of the system events are indicated. The values of the x_1 and x_2 at the

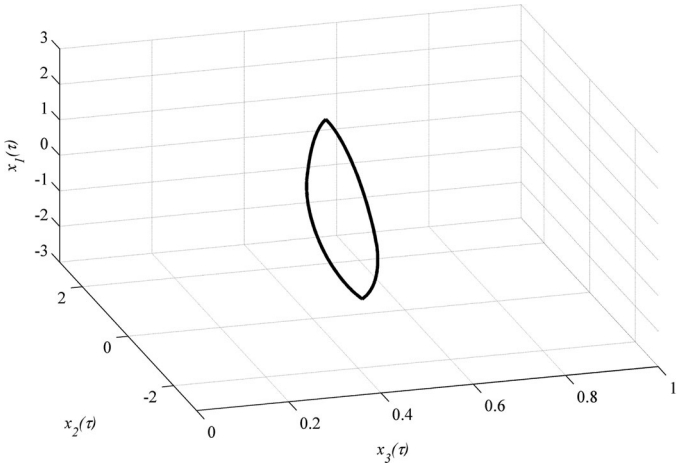

Fig. 5. Normalized state trajectory of a series-resonant converter in the steady state and above resonance.

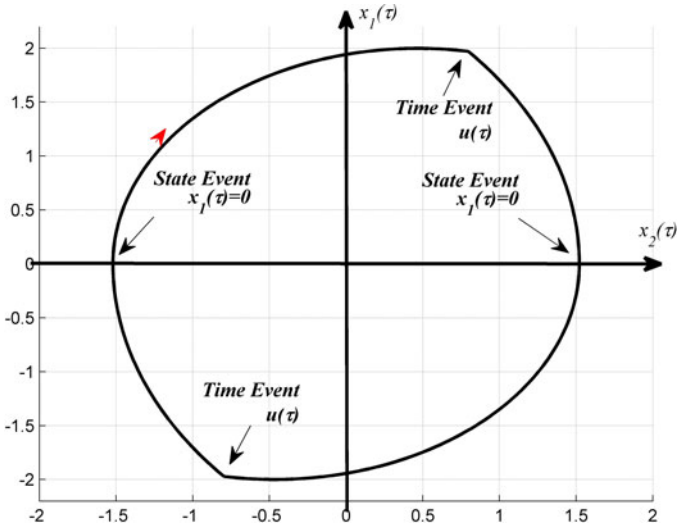

Fig. 6. Reduced-system phase-plane trajectory of the series-resonant converter with the system events locations.

time-event instant, using (10), could be written as

$$x_2(\gamma) = -x_2(0) = x_{3ss}x_{2p} \tag{11}$$

$$x_1(\gamma) = -x_1(0) = \sqrt{(1-x_{3ss}^2)x_{2p}(x_{2p}+2)}x_{2p} = \frac{x_{3ss}Q\gamma}{2} \tag{12}$$

where x_{2p} is the normalized maximum value of the resonant-tank capacitor voltage. In addition, from (9) with $k_m = 0$, (11), and (12), the slope of the switching surface can be obtained

$$k_n = \sqrt{\frac{(1-x_{3ss}^2)(x_{3ss}Q\gamma+4)}{x_{3ss}^3 Q\gamma}}. \tag{13}$$

So the control input of the series-resonant converter can be written in the form of (9), where $k_m = 0$ and k_n could be obtained by (13). The state-space representation of the system

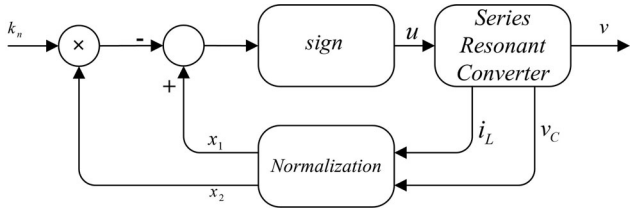

Fig. 7. Block diagram of the open-loop system with slope of the switching surface as the new control input.

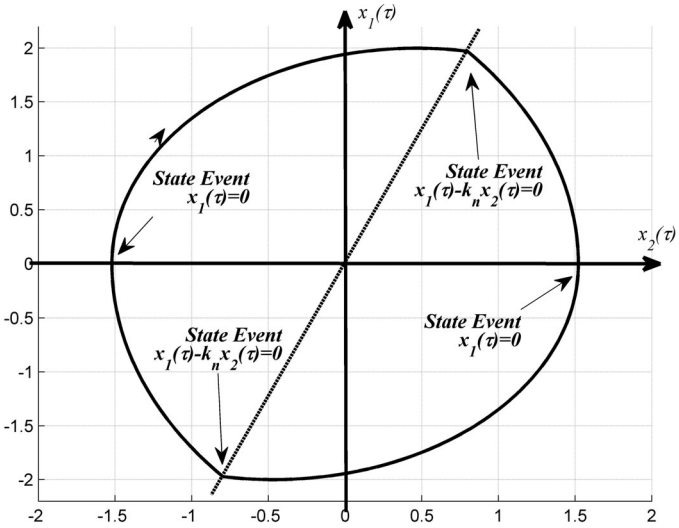

Fig. 8. Reduced-system phase-plane of the series-resonant converter with the proposed switching surface.

in (3) can be written as

$$\begin{aligned} \dot{x}_1 &= \text{sign}(x_1 - k_n x_2) - x_3\text{sign}(x_1) - x_2 \\ \dot{x}_2 &= x_1 \\ \alpha\dot{x}_3 &= |x_1| - x_3 Q. \end{aligned} \tag{14}$$

In (14), all events of the system transform to state events and it could be rewritten in the form of (6). The stability of the system in (6) can be considered by piecewise quadratic Lyapunov functions [18]. Furthermore, the control input of the system is changed from switching frequency to switching surface slope. The block diagram of (14) is plotted in Fig. 7, where slope of the switching surface is considered as control input. In Fig. 8, the locations of the state events in the PWA model are expressed and subsystems of system (14) in the PWA model are shown in Table I.

In Fig. 9, the system gain related to the switching surface slope is plotted for the series-resonant converters with different quality factors in the ideal case. Using Fig. 10 that illustrates the switching surface slope versus the normalized switching frequency ($F = \pi/\gamma$) and Fig. 9, the converter design pattern based on the switching surface slope could be successful for a specific quality factor. The series-resonant converter is designed for a prespecific switching frequency, output power, output voltage, and quality factor. The load resistance and the characteristic impedance of such a converter can be found using output power,

TABLE I
SERIES-RESONANT CONVERTER SUBSYSTEMS ASSOCIATED WITH THE PWA MODEL

System Mode: Conducting Switches	A_i	b_i	H_i^T , g_i
1: D_1 , D_4 , D_5 , D_8	$\begin{bmatrix} 0 & -1 & +1 \\ +1 & 0 & 0 \\ \frac{-1}{\alpha} & 0 & \frac{-Q}{\alpha} \end{bmatrix}$	$\begin{bmatrix} +1 \\ 0 \\ 0 \end{bmatrix}$	$g_i = \begin{bmatrix} 0 & 0 \end{bmatrix}^T$ $H_i = \begin{bmatrix} 1 & -1 \\ 0 & k_n \\ 0 & 0 \end{bmatrix}$
2: Q_1 , Q_4 , D_5 , D_8	$\begin{bmatrix} 0 & -1 & -1 \\ +1 & 0 & 0 \\ \frac{1}{\alpha} & 0 & \frac{-Q}{\alpha} \end{bmatrix}$	$\begin{bmatrix} +1 \\ 0 \\ 0 \end{bmatrix}$	$g_i = \begin{bmatrix} 0 & 0 \end{bmatrix}^T$ $H_i = \begin{bmatrix} -1 & -1 \\ 0 & k_n \\ 0 & 0 \end{bmatrix}$
3: D_2 , D_3 , D_6 , D_7	$\begin{bmatrix} 0 & -1 & -1 \\ +1 & 0 & 0 \\ \frac{1}{\alpha} & 0 & \frac{-Q}{\alpha} \end{bmatrix}$	$\begin{bmatrix} -1 \\ 0 \\ 0 \end{bmatrix}$	$g_i = \begin{bmatrix} 0 & 0 \end{bmatrix}^T$ $H_i = \begin{bmatrix} -1 & 1 \\ 0 & -k_n \\ 0 & 0 \end{bmatrix}$
4: Q_2 , Q_3 , D_6 , D_7	$\begin{bmatrix} 0 & -1 & +1 \\ +1 & 0 & 0 \\ \frac{-1}{\alpha} & 0 & \frac{-Q}{\alpha} \end{bmatrix}$	$\begin{bmatrix} -1 \\ 0 \\ 0 \end{bmatrix}$	$g_i = \begin{bmatrix} 0 & 0 \end{bmatrix}^T$ $H_i = \begin{bmatrix} 1 & 1 \\ 0 & -k_n \\ 0 & 0 \end{bmatrix}$

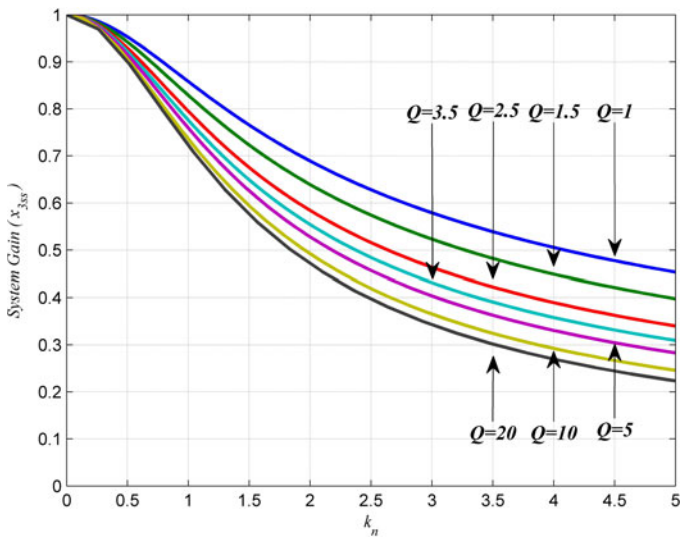

Fig. 9. Control-plane characteristic of the series-resonant converter above resonance, related to the switching surface slope, for different quality factors, in the ideal case.

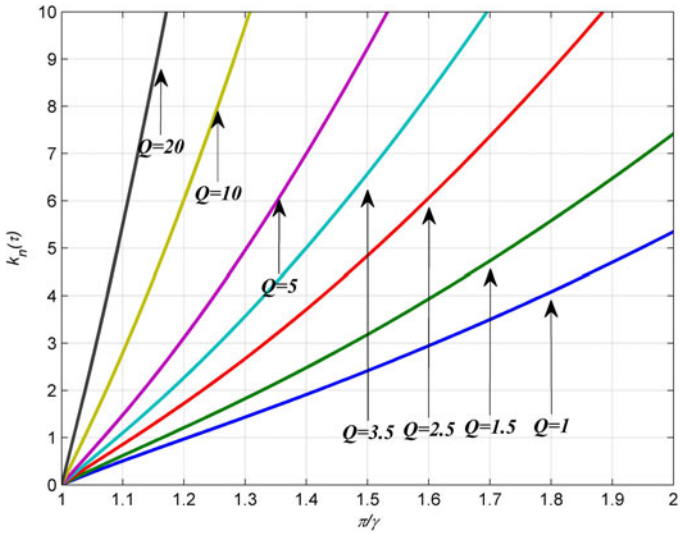

Fig. 10. Slope of the switching surface versus normalized switching frequency in the series-resonant converter, above resonance for different quality factors, in the ideal case.

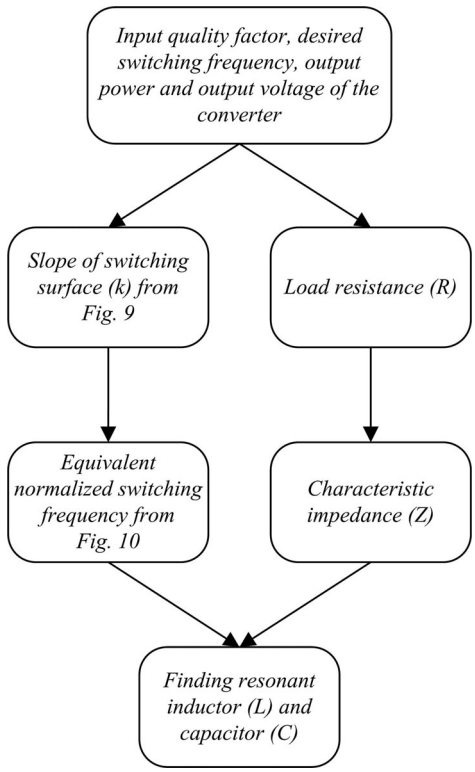

Fig. 11. Series-resonant converter design procedure in the above resonance based on the slope of the switching surface.

output voltage, and quality factor. The system gain (x_{3ss}) is brought by output voltage of the system. As a result, the slope of the switching surface can be found from Fig. 9. Finding resonant-tank parameter needs information about the normalized switching frequency that is shown in Fig. 10. These steps are summed up in a flow chart that can be seen in Fig. 11.

In this section, the problem of finding a switching frequency for a specific gain in a resonant converter has been transformed into the problem of finding a slope for the switching surface that can be solved graphically by Figs. 9 and 10 in the ideal case. The proposed method in this section for finding the series-resonant converter PWA model is in contrast to that in [9], in which first harmonic approximation is used to find the slope of switching surface. In addition, the property of the switching surface is defined based on the converter property and its phase plane which leads to solving a convex optimization problem in [9] that has different solutions for different convergence properties.

IV. Controller Synthesis

In the previous section, the series-resonant converter nonlinear model above resonance operation has been transformed into a PWA model. In the PWA model, the control input is the switching boundary slope. Before proposing the control law, it is appropriate to consider the effect of switching boundary slope variations on the output voltage. Because of the symmetrical operation of the system, half of the switching period is taken into consideration. In *Mode 2* [see Fig. 3(b)], switches Q_1 and Q_4 are turned ON and the inductor current is positive. The current flowing from the input voltage source V_g enters through the negative polarity, which is equivalent to energy production by V_g. Therefore, the energy level of the system is increased. When the switching constraint is satisfied, switches Q_1 and k_n are turned OFF, and due to the continuity of the inductor current, D_2 and D_3 start to conduct (*Mode 3*). In this mode, as can be seen in Fig. 3(c), the current of the input voltage source, V_g, enters through the positive polarity, which is equivalent to energy consumption by the input voltage source, and the energy level of the system is decreased. If the slope of the switching surface, k_n, is big enough, Q_1 and Q_4 conduction time and conduction interval of D_2 and D_3 remain almost the same. The energy transferred from the input voltage source to the system during the Q_1 and Q_4 conduction interval is almost equal to the energy transferred from the system to the input voltage source during the D_2 and D_3 conduction interval. In this situation, the output voltage approaches to zero. On the other hand, decreasing k_n leads to increasing the Q_1 and Q_4 conduction mode and the switches D_2 and D_3 conduction time approaches zero, which cause the transferred energy from the system to the input voltage source to tend to zero. The output voltage becomes the same as the input voltage, in the ideal case, for $k_n = 0$.

According to the contents, a control law for output voltage regulation could be obtained as follows. The nominal slope of the switching surface corresponding to the nominal operation of the series-resonant converter could be found from (13) or Fig. 9. The new value for k_n could be set by measuring the output voltage and comparing it with the reference voltage. If the output voltage is smaller than the reference voltage, the energy level of the system should be increased and k_n should be decreased. If the output voltage is greater than the reference voltage, then the energy level of the system should be decreased and k_n should be increased. A mathematical description for these statements can be expressed as

$$e = \frac{V_{\text{ref}} - v(t)}{V_g} \tag{15}$$

$$\dot{k} = -\psi \text{sign}(e) \tag{16}$$

where ψ is a positive constant to look at convergence property of the control law. The block diagram of the closed-loop system is shown in Fig. 10. As can be seen in this figure, the control system consists of two feedback loops. The inner loop includes the inductor current and the resonant-tank capacitor voltage which define the switching surface with the slope k_n. The outer loop calculates the error signal between the reference voltage and the output voltage. The error signal is applied to the controller block and the new value for k_n is achieved. In the next section, hardware implementation results of the proposed modeling method and control law are explained.

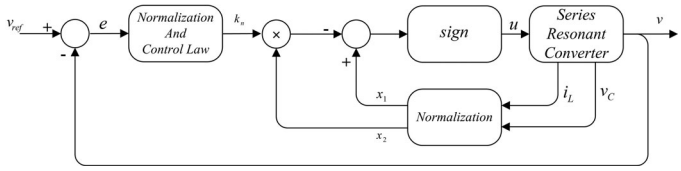

Fig. 12. Block diagram of the closed-loop system with the proposed controller for output voltage regulation based on switching surface slope adjustment.

V. Experimental Verification

The experimental setup includes a prototype series-resonant converter, a Yokogawa DL1540 oscilloscope for data logging, and a conventional PC. The oscilloscope is used to measure the normalized resonant inductor current, normalized resonant capacitor voltage, normalized output voltage, and the slope of the switching surface as control signal. To access the data, the oscilloscope was plugged into the PC.

A graphical interface was developed using National Instrument LabVIEW. This high-level language provides an easy way to export data from the oscilloscope to the PC in every test via the universal serial bus port. The data have been imported and plotted in MATLAB.

To evaluate the performance of the proposed model in (14), an experiment is conducted for a prototype series-resonant converter represented in Fig. 13. As can be seen from Fig. 13, the prototype board includes three main parts. The first part which is named "A" is the series-resonant converter with IRF740 and MBR20100 as full-bridge inverter power MOSFETs and rectifier diodes, respectively. The converter parameters are given in Table II. Using the values of the table for resonant inductor, resonant capacitor, and load resistor, the quality factor of the converter is $Q = 2.5$. According to Table II, input and output voltages of the converter are 14 and 30 V, respectively. Take into consideration forward voltage of the rectifier diodes effect on the output voltage result $x_{3ss} = 0.51$ for the converter gain. Using the content of Section III, this gain could be obtained by the slope of the switching surface $k_n = 2.5$. Corresponding switching frequency of the converter can be found using Fig. 10. From Fig. 10, the normalized switching frequency for the converter with $Q = 2.5$ and $k_n = 2.5$ is $F = 1.3$. The resonant frequency $f_o = 50$ kHz, in Table II, and $F = 1.3$ result $f_s = 65$ kHz for the switching frequency.

Power MOSFET driver's circuit is the second part in the prototype board, which is named "B" in Fig. 13, designed based on IR2110 driver. In Fig. 14, related circuits to the part "A" and "B" are illustrated.

To measure the state variables x_1, x_2 and feeding to the switching surface and control input production network (see Fig. 17), circuits shown in Figs. 15 and 16 have been used. Part "C" on prototype board in Fig. 13 is related to the measuring and normalization circuits and equipped with AD826 high-speed dual op-amps ICs.

TABLE II
PARAMETERS OF THE PROTOTYPE SERIES-RESONANT CONVERTER

Symbol	PARAMETERS	Quantity
L	Inductance	100 μH
C	Capacitance	100 nF
C_F	Capacitance	47 μF
R	Load resistance	12 Ω
V_g	Input voltage	30 V
V	Output voltage	14 V
$V_{\rm fw}$	Forward voltage of diodes	0.7 V
f_o	Resonant frequency	50 kHz

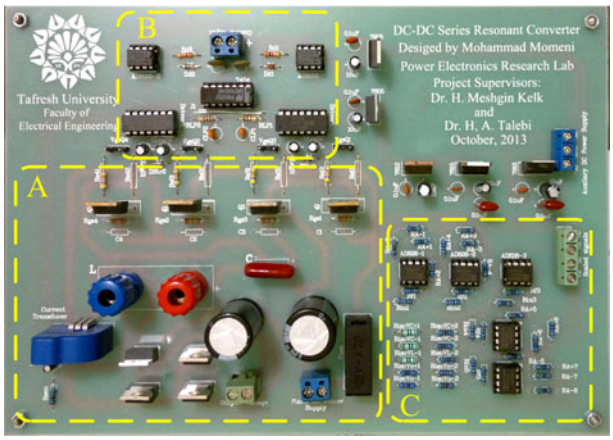

Fig. 13. Prototype series-resonant converter.

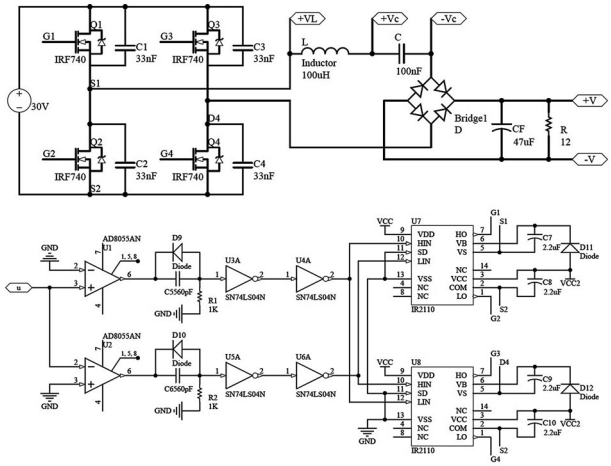

Fig. 14. Series-resonant converter implementation circuit with power MOSFET driver's based on IR2110.

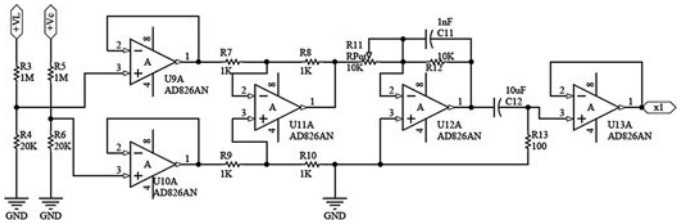

Fig. 15. Inductor current estimation and the normalization circuit.

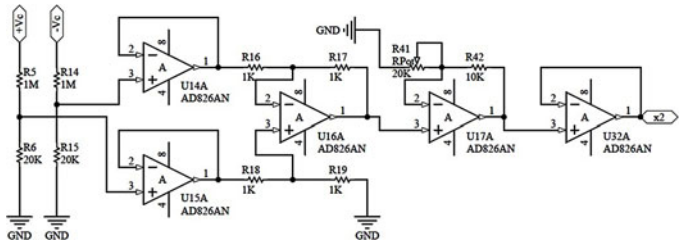

Fig. 16. resonant-tank capacitor voltage scaling circuit.

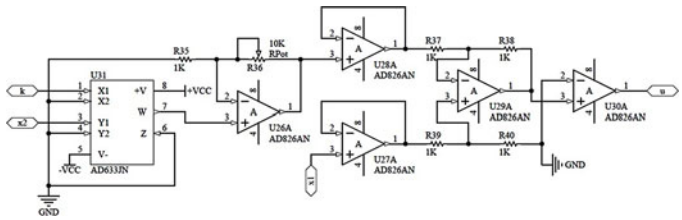

Fig. 17. Switching surface and control input circuit.

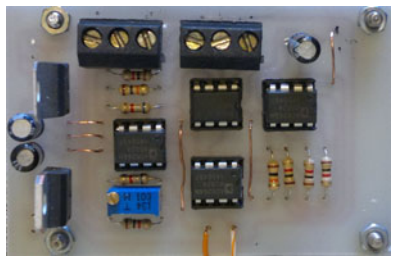

Fig. 18. Switching surface and control input production board.

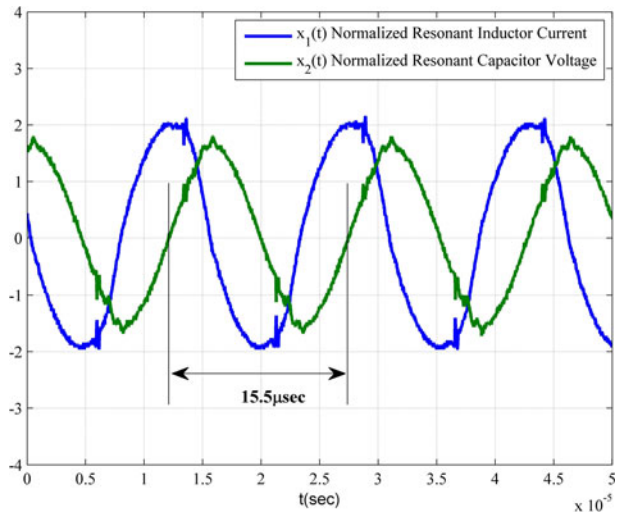

Fig. 19. Steady-state waveforms of the normalized inductor current and the normalized resonant capacitor voltage.

In Fig. 18, the switching surface production board is shown which benefits AD633 four-quadrant analog multiplier to produce control input signal.

The responses of x_1 and x_2, extracted from the prototype system in steady state, are depicted in Fig. 19 which shows

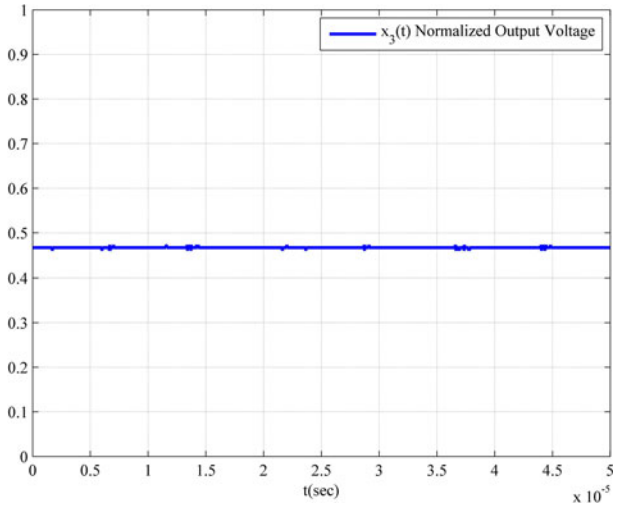

Fig. 20. Steady-state waveforms of the normalized output voltage for the slope of the switching surface $k_n = 2.5$.

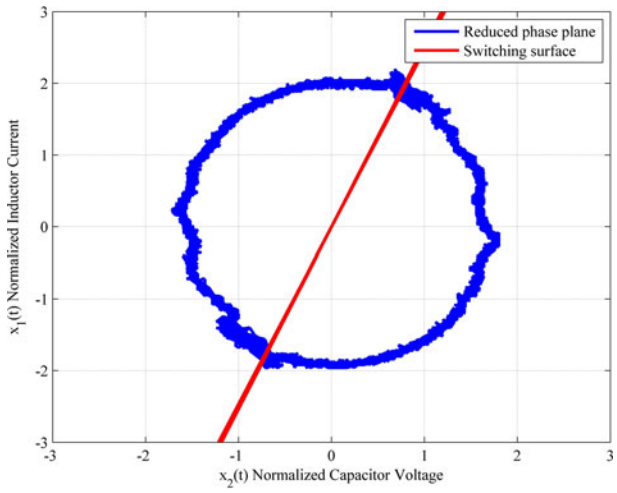

Fig. 21. Steady-state trajectory in the phase-plane and the proposed switching boundary.

$15.5-\mu$s length of a period for the resonant-tank state signals and results 64.5 kHz for the converter switching frequency. As can be seen from the figure, the converter is operated in CCM and above the resonant frequency. The time evaluation of the normalized output voltage x_3 and the phase-plane trajectory of the system with the proposed switching boundary in steady state are shown in Figs. 20 and 21, respectively. These figures indicate that the desired converter gain in Table II is satisfied by the related switching surface slope obtained from Fig. 9. Sampling frequency of the oscilloscope in this situation is 50×10^6 Samples/s.

For circuit implementation of the closed-loop system in Fig. 12, a scaling circuit for output voltage according to Fig. 22 has been employed. Moreover, to realize the controller law (16), the first-order transfer function has been used as follows:

$$G(s) = \frac{1}{1+0.1s}. \tag{17}$$

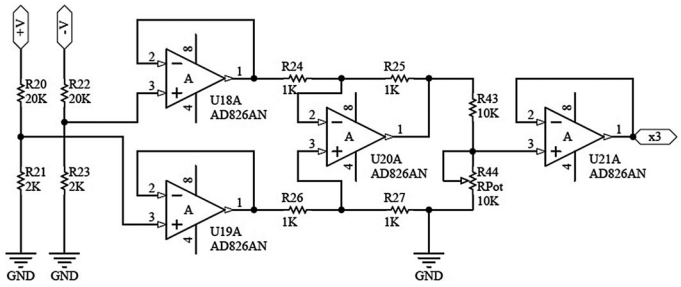

Fig. 22. Normalization circuit for the converter output voltage.

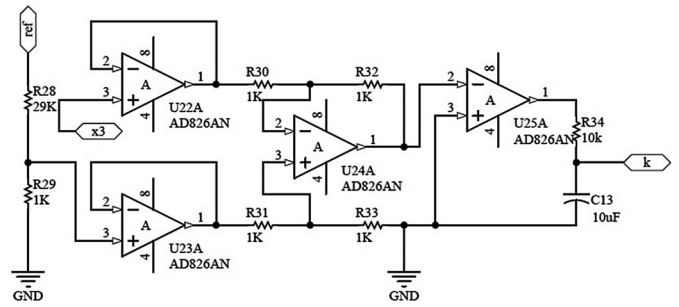

Fig. 23. Circuit-implementation of the controller with first-order transfer function for integrator.

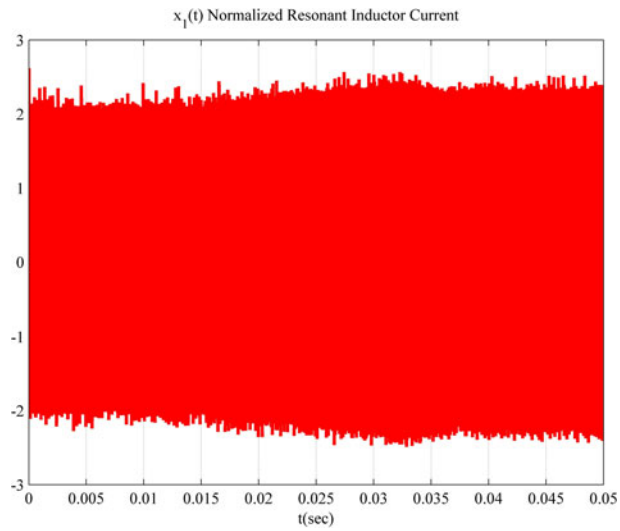

Fig. 24. Normalized inductor current, for a step-up change of the reference voltage.

Circuit implementation of the control law with a modified integrator transfer function in (17) is according to Fig. 23. For the performance verification of the proposed controller, three different experiments are conducted. Sampling frequency of the oscilloscope in these experiments is 200×10^3 Samples/s.

The first experiment considers the closed-loop system behavior in the presence of a step change in reference voltage from 14 to 16 V. In Figs. 24 and 25, the normalized inductor current and the normalized resonant-tank capacitor voltage for a rising

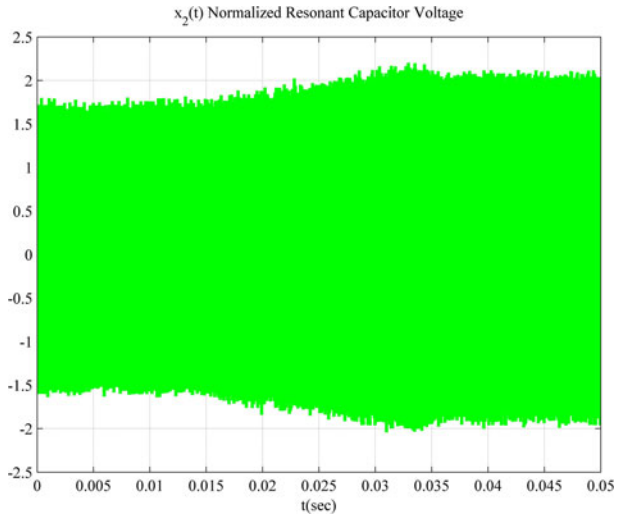

Fig. 25. Normalized resonant-capacitor voltage, for a step-up change of the reference voltage.

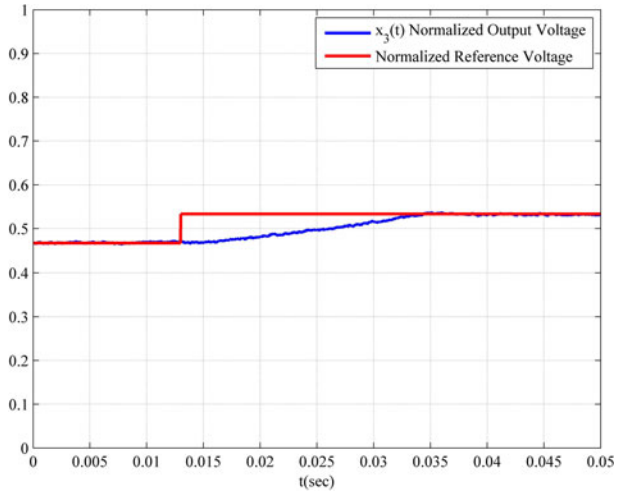

Fig. 26. Normalized output and reference voltages, for a step-up change of the reference voltage.

step change of the reference voltage are plotted, respectively. As can be seen, the amplitudes of the inductor current and the resonant-tank capacitor voltage have increased after the step-up change in the reference voltage. The normalized output voltage of the converter is shown in Fig. 26, which illustrates the output voltage that is tracking the reference voltage. Moreover, there is no overshoot in step responses of the closed-loop system which is an important point in voltage regulator systems. The controller output signal k_n is shown in Fig. 27 that decreases to boost the output voltage.

The second case to be analyzed is the closed-loop behavior when the load resistance abruptly changes from 12 to 8 Ω. In Figs. 28 and Fig. 29, the responses of the normalized inductor current and the resonant-tank capacitor voltage are depicted. As can be seen in Fig. 30, the output voltage approaches the reference one after the transient response within 25 ms. Fig. 31

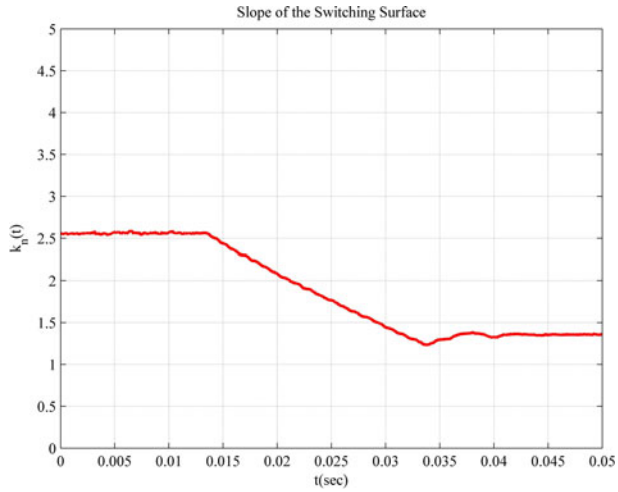

Fig. 27. Control signal k_n, for a step-up change of the reference voltage.

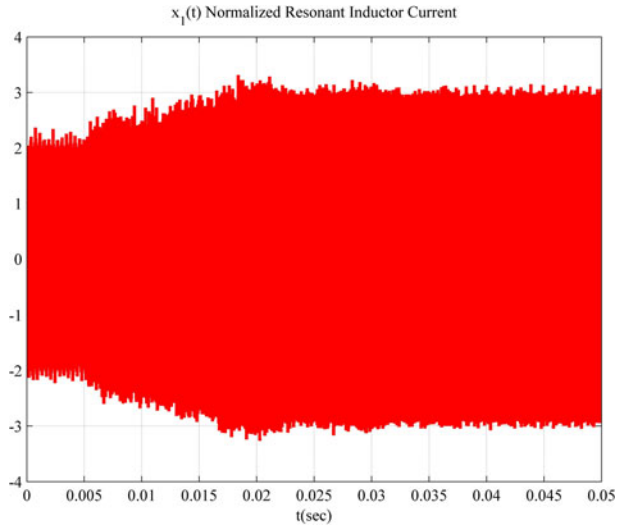

Fig. 28. Normalized inductor-current response, to a step-down change in the load resistance.

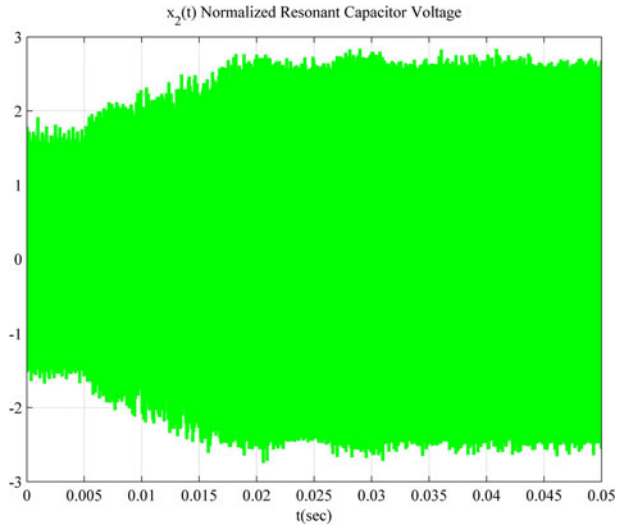

Fig. 29. Normalized resonant-capacitor voltage response, to a step-down change in the load resistance.

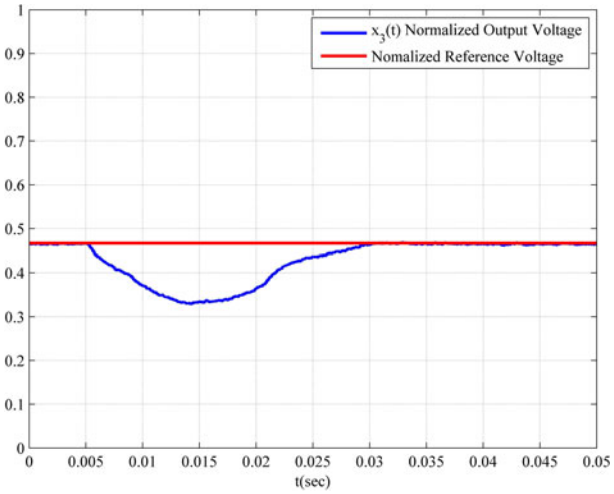

Fig. 30. Dynamic response of the normalized output voltage, to a step-down change in the load resistance.

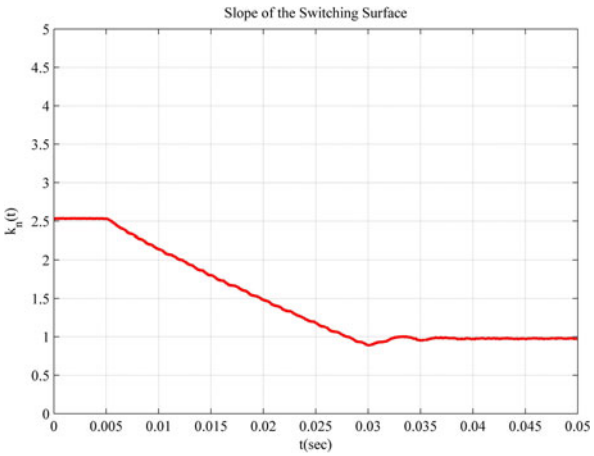

Fig. 31. Control signal k_n, for a step-down change in the load resistance.

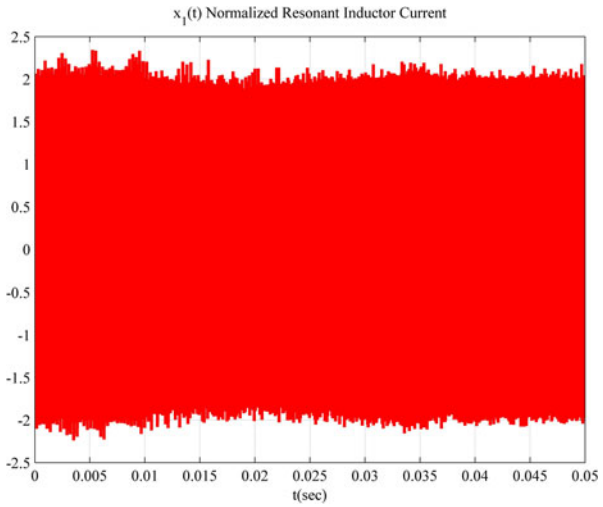

Fig. 32. Normalized inductor current response to a step-down change of the input-source voltage.

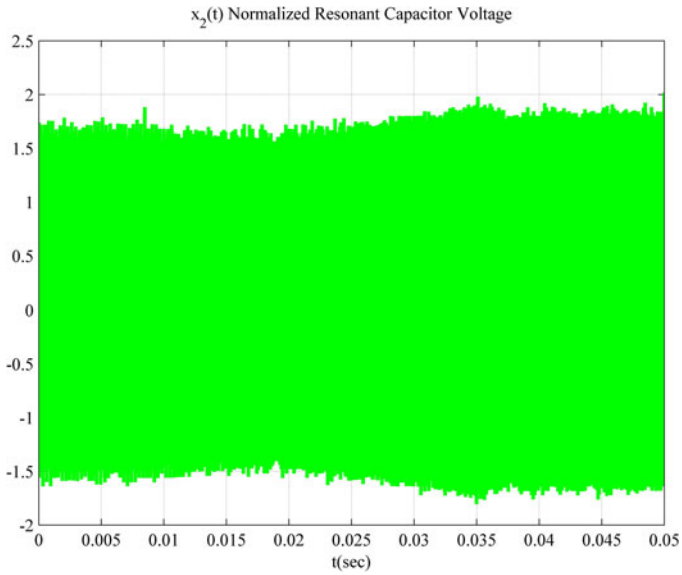

Fig. 33. Normalized resonant-capacitor voltage response, to a step-down change of the input-source voltage.

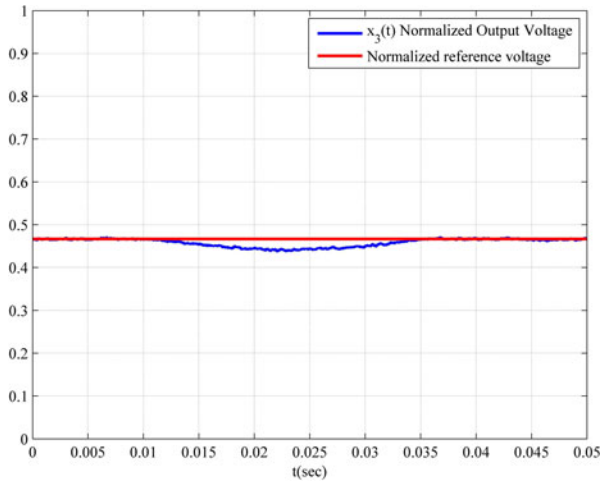

Fig. 34. Dynamic response of the normalized output voltage, to a step-down change of the input-source voltage.

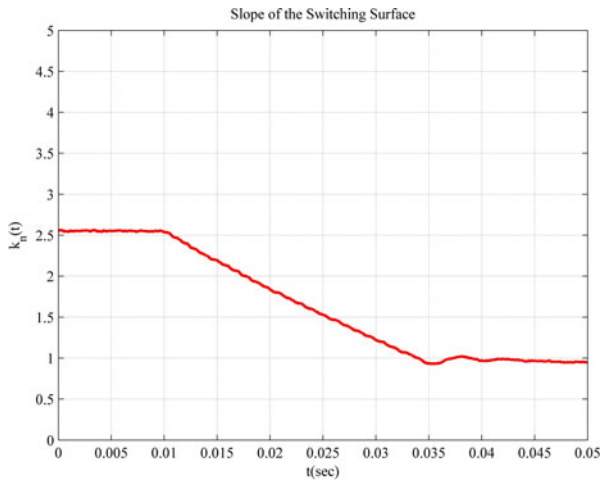

Fig. 35. Variation of control signal k_n for a step-down change of the input-source voltage.

illustrates the controller action that compensates the slope of the switching surface and causes the output voltage to follow the reference voltage.

The third experiment concerns a 16.67% decrement in the input-source voltage in the steady-state operation. In Figs. 32 and 33, the normalized inductor current and the normalized resonant-tank capacitor voltage are shown, respectively. The normalized output voltage of the converter is plotted in Fig. 34, which illustrates that the reference voltage was tracked by the output voltage after transient response interval. The controller operation in Fig. 35 shows the slope of the switching surface which is adjusted in such a way that the output voltage reaches its desired value after approximately 25 ms.

VI. Conclusion

A new modeling and control approach for the series-resonant converter has been presented using switched systems methodology. More specifically, control characteristic of the series-resonant converter based on the switching surface slope has been obtained for different quality factors.

The key idea of a rotating switching surface has been employed to control a series-resonant converter. The method is presented here for the series-resonant converter; however, it could be extended to other converters configurations as well. The proposed controller has some desirable properties such as robustness under load and input voltage variations and easy implementation. Online computation of the control signal does not need a heavy computation and makes the proposed approach applicable for real-time and high-frequency applications.

References

[1] R. W. Erickson and D. Maksimovic, *Fundamentals of Power Electronics*, 2nd ed. Norwell, MA, USA: Kluwer, 2001.

[2] R. Priewasser, M. Agostinelli, C. Unterrieder, S. Marsili, and M. Huemer, "Modeling, control, and implementation of DC–DC converters for variable frequency operation," *IEEE Trans. Power Electron.*, vol. 29, no. 1, pp. 287–301, Jan. 2014.

[3] S. R. Sanders, J. M. Noworolski, X. Z. Liu, and G. C. Verghese, "Generalized averaging method for power conversion circuits," *IEEE Trans. Power Electron.*, vol. 6, no. 2, pp. 251–259, Apr. 1991.

[4] Y. Yin, R. Zane, J. Glaser, and R. Erickson, "Small-signal analysis of frequency-controlled electronic ballasts," *IEEE Trans. Circuits Syst. I, Fundam. Theory Appl.*, vol. 50, no. 8, pp. 1103–1110, Aug. 2003.

[5] J. Lunze and F. Lamnabhi-lagarrigue, *Handbook of Hybrid Systems Control*. New York, NY, USA: Cambridge Univ. Press, 2009.

[6] S. Mariéthoz, S. Almér, M. Bâja, A. G. Beccuti, D. Patino, A. Wernrud, J. Buisson, H. Cormerais, T. Geyer, H. Fujioka, U. Jönsson, C. Kao, M. Morari, G. Papafotiou, A. Rantzer, and P. Riedinger, "Comparison of hybrid control techniques for buck and boost DC-DC converters," *IEEE Trans. Control Syst. Technol.*, vol. 18, no. 5, pp. 1126–1145, Sep. 2010.

[7] P. Karamanakos, T. Geyer, and S. Manias, "Direct voltage control of DC–DC boost converters using enumeration-based model predictive control," *IEEE Trans. Power Electron.*, vol. 29, no. 2, pp. 968–978, Apr. 2013.

[8] F. Tahami and B. Molaei, "Piecewise affined system modeling and control of PWM converters," *J. Circuits, Syst. Comput.*, vol. 16, no. 1, pp. 113–128, Feb. 2007.

[9] H. Molla-Ahmadian, A. Karimpour, N. Pariz, and F. Tahami, "Hybrid modeling of a DC–DC series resonant converter: Direct piecewise affine approach," *IEEE Trans. Circuits Syst. I, Fundam. Theory Appl.*, vol. 18, no. 5, pp. 3112–3120, Jul. 2012.

[10] M. Carrasco, E. Galvan, G. Escobar, R. Ortega, and A. M. Stankovic, "Analysis and experimentation of nonlinear adaptive controllers for the series resonant converter," *IEEE Trans. Power Electron.*, vol. 15, no. 3, pp. 536–544, May 2000.

[11] J. M. Burdío, L. A. Barragán, F. Monterde, D. Navarro, and J. Acero, "Asymmetrical voltage-cancellation control for full-bridge series resonant inverters," *IEEE Trans. Power Electron.*, vol. 19, no. 2, pp. 461–469, Mar. 2004.

[12] J. T. Matysik, "A new method of integration control with instantaneous current monitoring for class D series-resonant converter," *IEEE Trans. Ind. Electron.*, vol. 53, no. 5, pp. 1564–1576, Oct. 2006.

[13] L. R. Nerone, "Auto switching LED driver," *IEEE Trans. Power Electron.*, vol. 27, no 8, pp. 3834–3842, Aug. 2012.

[14] J. M. Alonso, M. S. Perdigao, D. G. Vaquero, A. J. Calleja, and E. S. Saraiva, "Analysis, design and experimentation on constant frequency DC–DC resonant converters with magnetic control," *IEEE Trans. Power Electron.*, vol. 27, no. 3, pp. 1369–1382, Mar. 2012.

[15] V. Hernandez Guzman, "A new stability analysis for dc-dc series resonant converter," *J. Comput. Syst.*, vol. 11, no. 1, pp. 14–27, Oct. 2007.

[16] H. S. Witsenhausen, "A class of hybrid-state continuous time dynamic systems," *IEEE Trans. Autom. Control*, vol. 11, no. 2, pp. 161–167, Apr. 1966.

[17] S. LeBel and L. Rodrigues, "PWL and PWA H_∞ controller synthesis for uncertain PWA slab systems: LMI approach," *Int. J. Control*, vol. 82, no. 3, pp. 482–492, 2009.

[18] L. Rodrigues and S. P. Boyd, "Piecewise-affine state feedback for piecewise-affine slab systems using convex optimization," *Syst. Control Lett.*, vol. 54, no. 9, pp. 835–853, 2005.

Mohammad Momeni received the Diploma degree in mathematics and physics from Alborz High School, Tehran, Iran, in 2004, and the B.Sc. degree in electronics from Khorasan Institute of Higher Education, Iran, in 2009, when he patented three Iranian inventions. He received the M.Sc. degree in control (third class student) from Tafresh University, Tafresh, Iran, in 2013.

He was with the Abzar Azma Company as a Research Engineer where he was working on power converters modeling and control, from 2009 to 2010. Although he was working on target-tracking systems, his research interests include control, hybrid, and switched systems, fuzzy control, and dc–dc power conversion systems.

Homayoun Meshgin Kelk received the B.Sc. degree from the Isfahan University of Technology, Isfahan, Iran, in 1987, and the M.Sc. and Ph.D. degrees in power engineering from Amirkabir University of Technology, Tehran, Iran, in 1991 and 2000, respectively.

He is currently an Assistant Professor and the Head of the Electrical Engineering Department at Tafresh University, Tafresh, Iran. In 2000, he was a Visiting Scholar in the Department of Electrical Engineering, Texas A&M University, College Station, TX, USA. His research interests include power electronics, modeling, and fault diagnosis of electrical machines.

Heidarali Talebi (M'02–SM'08) received the B.Sc. degree in electronics from Ferdowsi University, Mashhad, Iran, in 1988, the M.Sc. degree in electronics (first class honors) from Tarbiat Modarres University, Tehran, Iran, in 1991, and the Ph.D. degree in electrical and computer engineering from Concordia University, Montreal, QC, Canada, in 1997.

He held several postdoctoral and research positions at Concordia University and the University of Western Ontario, London, ON, Canada, before joining Amirkabir University of Technology, Tehran, in 1999, where he holds an Associate Professor position. He also served as the Head of the Control Systems Group at Amirkabir University from 2002 to 2004. He currently serves as a Research Deputy in the Department of Electrical Engineering, Amirkabir University of Technology. His research interests include control, robotics, fault diagnosis and recovery, intelligent systems, adaptive control, nonlinear control, and real-time systems.